A Femtosecond Study of Excitation Wavelength Dependence of a Triblock Copolymer−Surfactant Supramolecular Assembly: $(PEO)_{20}-(PPO)_{70}-(PEO)_{20}$ and CTAC

Shantanu Dey, Aniruddha Adhikari, Ujjwal Mandal, Subhadip Ghosh, and Kankan Bhattacharyya*

Physical Chemistry Department, Indian Association for the Cultivation of Science, Jadavpur, Kolkata 700 032, India

Received: January 10, 2008

Solvation dynamics and anisotropy decay of coumarin 480 (C480) in a supramolecular assembly containing a triblock copolymer, $PEO_{20}-PPO_{70}-PEO_{20}$ (Pluronic P123) and a surfactant, CTAC (cetyl trimethylammonium chloride) are studied by femtosecond up-conversion. In a P123−CTAC complex, C480 displays a significant (22 nm) red edge excitation shift (REES) in the emission maximum as λ_{ex} increases from 335 to 445 nm. This suggests that the P123−CTAC aggregate is quite heterogeneous. The average rotational relaxation time ($\langle\tau_{rot}\rangle$) of C480 in a P123−CTAC complex decreases by a factor of 2 from 2500 ps at $\lambda_{ex} = 375$ nm to 1200 ps at $\lambda_{ex} = 435$ nm. For $\lambda_{ex} = 375$ nm, the probe molecules in the buried core region of P123−CTAC are excited and the solvation dynamics displays three components, 2, 60, and 4000 ps. It is argued that insertion of CTAC in P123 micelle affects the polymer chain dynamics, and this leads to reduction of the 130 ps component of P123 micelle to 60 ps in P123−CTAC. For $\lambda_{ex} = 435$ nm, which selects the peripheral highly polar corona region, solvation dynamics in P123−CTAC and P123 are extremely fast with a major component of <0.3 ps (∼80%) and a 2 ps (∼20%) component.

1. Introduction

Water soluble triblock copolymers display interesting structures and rich diversity in phases and have versatile industrial applications.[1−9] In $(PEO)_{20}-(PPO)_{70}-(PEO)_{20}$ (Pluronic P123), the PEO block is highly hydrophilic while the PPO block is extremely hydrophobic and insoluble in water above 288 K.[1] At a temperature above 288 K, dehydration of the PPO blocks leads to the formation of a P123 micelle with a hydrophobic core (PPO block) of radius ∼5.8 nm and a hydrophilic corona (PEO) of thickness 4.2 nm (Scheme 1A).[1−3,8a] From Scheme 1A, it is evident that a tri-block copolymer micelle is highly heterogeneous on a molecular length scale and a fluorescent probe of length ∼1 nm should reveal the heterogeneity. However, some of the recent studies on solvation dynamics[4b−c] and isomerization[4d] did not attempt to delineate the dynamics in different regions of the triblock copolymer micelle. Castner and co-workers studied anisotropy decay in different regions of such a micelle using fluorescent probes with varying hydrophobicity.[5a−b] In order to study picosecond solvation dynamics in different regions of an amphiphilic di-block copolymer, Hof and co-workers decomposed the emission spectra into two subspectra and attempted to monitor their time evolution separately.[4a] Though this method is quite logical, it involves too many parameters and is often very difficult to separately monitor the contributions of the different subspectra.

Recently, we studied dynamics in different regions of a P123 micelle,[6a] P123 gel,[6b] and P123−SDS aggregate[6c] by varying the excitation wavelength (λ_{ex}) using femtosecond up-conversion. Excitation at a shorter wavelength ("blue edge") selects a solvatochromic probe (e.g., coumarin 480, C480) in a relatively nonpolar environment (e.g., PPO block) and gives rise to a blue-shifted emission spectrum. On the contrary, excitation at a longer wavelength ("red edge") selects the probe residing at a relatively polar environment (PEO block) and gives rise to a red-shifted emission spectrum. This is known as red edge excitation shift (REES).[10] Thus, one may spatially resolve dynamics in different regions of a heterogeneous system by variation of the excitation wavelength (λ_{ex}). We have demonstrated this by studying λ_{ex} dependence of solvation dynamics in the micellar[6a] and gel[6b] phase of a P123 micelle in a P123−SDS aggregate[6c] and in a reverse micelle containing an ionic liquid[6d] and also in the case of FRET in a reverse micelle[7a] and P123 micelle.[7b]

SCHEME 1: Schematic Representation of (A) P123 Micelle and (B) Coumarin 480 (C480)

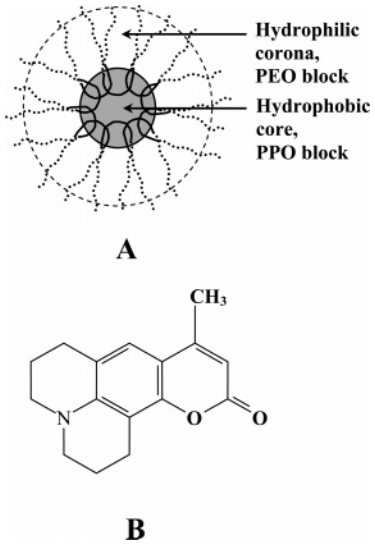

* Corresponding author. E-mail: pckb@mahendra.iacs.res.in. Fax: (91)-33-2473-2805.

10.1021/jp8002257 CCC: $40.75
Published on Web 04/03/2008

The interaction of the neutral triblock copolymers P123 with ionic surfactants results in the formation of supramolecular assemblies. Such assemblies have been studied using SANS, NMR, dynamic light scattering, fluorescence, and calorimetry.[8−9] According to a SANS study, P123 forms different kinds of complexes with cetyl trimethylammonium chloride (CTAC) depending on the molar ratio of CTAC and P123.[8a] At a CTAC/P123 molar ratio of ≤0.5, the micelle is rich in P123 with a few CTAC monomers associated noncooperatively with the P123 micelle. At a CTAC/P123 molar ratio of ∼0.3, both the core and overall radius are smaller than those in P123 micelle by ∼1 nm (core radius ∼ 3.5 nm and overall radius ∼ 9 nm).[8a] In the presence of excess CTAC (CTAC−P123 molar ratio of ≥1.9), the micellar structure of P123 breaks giving rise to two types of complexes, one P123−rich and the other CTAC-rich.[8a] In the present work, we focus our attention on how penetration of a P123 micelle by CTAC affects solvation dynamics and anisotropy decay. To ensure that only one kind of assembly is present, we used low CTAC/P123 molar ratio (0.3) and CTAC at a concentration 0.5 mM, which is much lower than its cmc (1.3 mM).[11]

Before we proceed, we note that the present system (P123−CTAC) differs in a number of ways from the P123−SDS system, studied earlier.[6c] First, in the P123−SDS system, the surfactant (SDS) is larger in number (P123:SDS = 1:5). In P123−CTAC aggregate, the surfactant (CTAC) is fewer in number (P123:CTAC = 3:1). Second, penetration of the core of P123 by a large number of SDS molecules reduces the difference between the core (PPO block) and corona region (PEO) and, hence, a small REES (5 nm). In P123−CTAC, the difference between the core and the corona is quite large and this results in a large REES (22 nm) similar to P123 micelle. Third, the P123 concentration used (10 wt %) in the case of P123−SDS is 10 times higher than that used (1 wt %) for P123−CTAC. We will see later that this reduces the contribution of the chain dynamics to the solvation dynamics in the case of P123−CTAC compared to that in P123−SDS. We will discuss this and other differences in the solvation dynamics and anisotropy decay for these two systems.

2. Experimental

The triblock copolymer, Pluronic P123 (P123) (Scheme 1A) was a gift from BASF Corporation and was used without further purification. Coumarin 480 (C480, Scheme 1B) was purchased from Exciton. Highly purified cetyl trimethylammonium chloride (CTAC) was prepared from cetyl trimethylammonium bromide (CTAB, 0.3 g, 0.82 mM) by ion exchange chromatography using Amberlyst A-26 chloride resin. The eluent (chloroform/methanol, 1:1, v/v) was removed on a rotary evaporator followed by drying in a high-vacuum pump. Pure CTAC was obtained by crystallizing the solid residue thrice from methanol/ether. The yield of the white crystalline product was ∼90%.

The copolymer solution was prepared by mixing proper amount of the copolymer (P123) with 100 mL water. The solution was stirred for 4−5 h using a magnetic stirrer at room temperature in a sealed container. We used 1 wt % P123 (∼1.74 mM), and 0.5 mM CTAC so as to keep the CTAC/P123 molar ratio at ∼0.3. At 0.5 mM CTAC (far below the critical micelle concentration, cmc ∼1.3 mM),[11] formation of CTAC micelles is avoided. All experiments were performed at room temperature (∼25 °C).

The steady state absorption and emission spectra were recorded in a Shimadzu UV-2401 spectrophotometer and a Spex FluoroMax-3 spectrofluorimeter, respectively.

In our femtosecond up-conversion setup (FOG 100, CDP), the sample was excited at 375, 405, and 435 nm using the second harmonic of a mode-locked Ti-sapphire laser with an 80 MHz repetition rate (Tsunami, Spectra Physics), pumped by 5 W Millennia (Spectra Physics). The fundamental beam was frequency doubled in a nonlinear crystal (1 mm BBO, $\theta = 25°$, $\phi = 90°$). The fluorescence emitted from the sample was up-converted in a nonlinear crystal (0.5 mm BBO, $\theta = 38°$, $\phi = 90°$) using a gate pulse of the fundamental beam. The up-converted light is dispersed in a monochromator and detected using photon counting electronics. A cross-correlation function obtained using the Raman scattering from ethanol displayed a full width at half-maximum (fwhm) of 350 fs. The femtosecond fluorescence decays were fitted using a Gaussian shape for the exciting pulse.

To fit the femtosecond data, one needs to know the long decay components. These were detected using a picosecond set up in which the samples were excited at 375, 405, and 435 nm using picosecond laser diodes (IBH Nanoleds) in an IBH Fluorocube apparatus. The emission was collected at a magic angle polarization using a Hamamatsu microchannel plate (MCP) photomultiplier (5000U-09). The time correlated single photon counting (TCSPC) setup consists of an Ortec 9327 CFD and a Tennelec TC 863 TAC. The data is collected with a PCA3 card (Oxford) as a multichannel analyzer. The typical fwhm of the system response using a liquid scatterer is about 90 ps. The fluorescence decays were deconvoluted using IBH DAS6 software. In order to fit the femtosecond transients, we first determined the long picosecond components by deconvolution of the picosecond decays. Then, the long picosecond components were kept fixed to fit the femtosecond data. During our previous study[6a] on 1 wt % P123, we did not have a picosecond laser diode at 435 nm and the fitting procedure was different. Thus the numbers reported here are slightly different.

The time-resolved emission spectra were constructed using the parameters of best fit to the fluorescence decays and the steady-state emission spectrum following the procedure described by Maroncelli and Fleming.[12a] The solvation dynamics is described by the decay of the solvent correlation function $C(t)$, defined as

$$C(t) = \frac{\nu(t) - \nu(\infty)}{\nu(0) - \nu(\infty)} \tag{1}$$

where $\nu(0)$, $\nu(t)$, and $\nu(\infty)$ are the peak frequencies at time 0, t, and ∞, respectively. Note, a portion of solvation dynamics is missed (at $\lambda_{ex} = 405$ and 435 nm) even in our femtosecond setup of time resolution of 350 fs. The amount of solvation missed is calculated using the Fee-Maroncelli procedure.[12b] In this method, the emission frequency at time zero, $\nu^{p}_{em}(0)$, may be calculated using the absorption frequency (ν^{p}_{abs}) in a polar medium (i.e., C480 in P123−CTAC complex) as

$$\nu^{p}_{em}(0) = \nu^{p}_{abs} - (\nu^{np}_{abs} - \nu^{np}_{em}) \tag{2}$$

where ν^{np}_{em} and ν^{np}_{abs} denote the steady-state frequencies of emission and absorption, respectively, of the probe (C480) in a nonpolar solvent (i.e., cyclohexane).

In order to study fluorescence anisotropy decay, the analyzer was rotated at regular intervals to get perpendicular ($I_{\perp}$) and parallel ($I_{||}$) components. Then the anisotropy function, $r(t)$ was calculated using the formula

$$r(t) = \frac{I_{||}(t) - GI_{\perp}(t)}{I_{||}(t) + 2GI_{\perp}(t)} \tag{3}$$

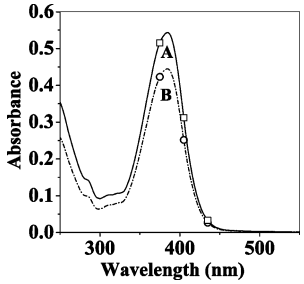

Figure 1. Absorption spectra of C480 in 1 wt % P123: (A) in the absence of CTAC (—) and (B) in the presence of 0.5 mM CTAC (-·--·). The excitation wavelengths are marked (□,○) at 375, 405, and 435 nm.

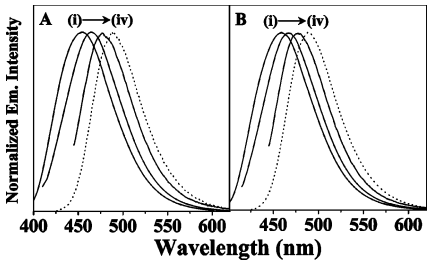

Figure 2. Emission spectra of C480 in 1 wt % P123 when excited at (i) 375 nm, (ii) 405 nm, (iii) 435 nm, and (iv) C480 in water (·····) (λ_{ex} = 375−435 nm): (A) without CTAC and (B) with 0.5 mM CTAC.

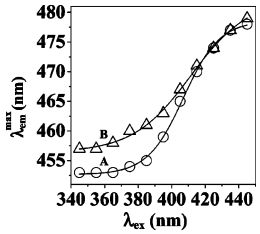

Figure 3. Plot of emission maximum of C480 in 1 wt % P123 as a function of excitation wavelength: (A) in the absence of CTAC (○) and (B) in the presence of 0.5 mM CTAC (△).

The *G* value of the picosecond setup was determined using a probe whose rotational relaxation is very fast, e.g., coumarin 480 in methanol. The *G* value was found to be 1.5.

3. Results

3.1. Steady-State Absorption and Emission Spectra: λ_{ex} Dependence. In a P123 micelle (1 wt %), the absorption maximum of C480 is at 380 nm (Figure 1) which is almost identical with that of C480 in acetonitrile[13] and is blue-shifted by 16 nm from that (396 nm)[13] in water. On addition of CTAC, the absorption maximum of C480 undergoes a slight red shift (Figure 1) to 384 nm. This is intermediate between the absorption peak in acetonitrile (380 nm) and in ethanol (387 nm).[13]

Emission spectra of C480 in both the P123 micelle and the P123−CTAC complex depend markedly on λ_{ex}. Panels A and B of Figure 2 show the emission spectra of C480 in P123 micelle and P123 micelle−CTAC aggregate at different λ_{ex}, respectively. Figure 3 shows the λ_{ex} dependence of emission maximum of coumarin 480 in P123 micelle−CTAC aggregate and in P123 micelle.

In the absence of CTAC, emission maximum of C480 in P123 micelle shows a 25 nm shift (REES) from 453 nm at λ_{ex} = 345 to 478 nm at λ_{ex} = 445 nm.[6a] On addition of CTAC, the REES becomes slightly smaller (22 nm) and the emission maximum shifts from 457 nm at λ_{ex} = 345 to 479 nm at λ_{ex} = 445 nm (Table 1). Note, the magnitude of REES in P123−CTAC is larger than that (5 nm) in P123−SDS.

TABLE 1: Excitation Wavelength Dependence of the Emission Maximum and fwhm of C480 in P123 (1 wt %) Micelle in the Presence and Absence of 0.5 mM CTAC

	λ_{em}^{max} (nm)			fwhm (cm^{-1})[a]		
λ_{ex} (nm)	P123	P123 + CTAC	water	P123	P123 + CTAC	water
375	455	460	489	3550	3550	2650
405	465	467	489	3400	3310	2650
435	477	477	489	2850	2920	2650

[a] ± 5%.

The red shift in the emission maximum of C480 in P123−CTAC complex (at λ_{ex} = 375 nm) compared to that in P123 micelle suggests that penetration of the ionic CTAC inside the P123 micelle increases local polarity of the core region (selected at λ_{ex} = 375 nm). Interestingly, excitation at the red end (λ_{ex} = 435 nm) exhibits very little red shift. This indicates that excitation at the red end selects the probe at the peripheral region (excited at λ_{ex} = 375 nm), which is quite exposed to bulk water both in P123 micelle and in P123−CTAC aggregate.

The magnitude of REES detected in the present work for P123−CTAC (22 nm) is much larger than that reported for a P123−SDS aggregate (5 nm).[6c] The very large REES of C480 in P123−CTAC complex indicates that the P123−CTAC assembly is more heterogeneous than the P123−SDS system. The larger REES in the case of P123−CTAC may be attributed to the larger size (R ∼ 9 nm)[8a] compared to that in P123−SDS (R ∼ 5 nm).[9] The similarity in REES and size of P123−CTAC aggregate with those of P123 micelle suggests that they are structurally similar and penetration of CTAC does not modify the overall structure of P123 to a large extent.

At all $\lambda_{ex,}$ the full width at half-maximum (fwhm) in P123 micelle−CTAC aggregate is very similar to that in P123 micelle and is larger than that in P123−SDS aggregate (Table 1). The fwhm values in P123 micelle are 3550, 3400, and 2850 cm^{-1} for λ_{ex} = 375, 405, and 435 nm, respectively. The corresponding values for P123 micelle−CTAC aggregate are, respectively, 3550, 3310, and 2920 cm^{-1} and for P123−SDS aggregate are, respectively, 3100, 2900, and 2650 cm.$^{-1}$ Note, fwhm of the emission spectrum of C480 in water is relatively smaller (2650 cm^{-1}) and is independent of λ_{ex}. The relatively large fwhm and its λ_{ex} dependence also implies a heterogeneous structure of P123−CTAC and P123 micelle.

3.2. Fluorescence Anisotropy Decay of C480 in P123 Micelle and P123−CTAC Aggregate. The time constant of fluorescence anisotropy decay of C480 in bulk water is 70 ps.[14] The fluorescence anisotropy decay of C480 in P123 and in P123/CTAC complex (at the blue side of the emission peak) is found to be much slower and is biexponential

$$r(t) = r_0 [\beta \exp(-t/\tau_{slow}) + (1 - \beta) \exp(-t/\tau_{fast})] \quad (4)$$

In a P123 micelle, the anisotropy decay of C480 for λ_{ex} = 375 nm is described by two components: 450 ps (25%) and 2750 ps (75%) (Figure 4, Table 2). At λ_{ex} = 435 nm, the observed components are 400 ps (75%) and 2050 ps (25%). Thus the average rotational relaxation time ($\langle\tau_{rot}\rangle$) decreases ∼3 times from ∼2200 ps at λ_{ex} = 375 nm to 800 ps at λ_{ex} = 435 nm. The faster rotational dynamics at longer λ_{ex} indicates lower microscopic friction for probes in the peripheral and highly polar region (selected at λ_{ex} = 435 nm) compared to that in the core.

In a P123−CTAC aggregate, for λ_{ex} = 375 nm, the components of the anisotropy decay of C480 are 630 ps (35%)

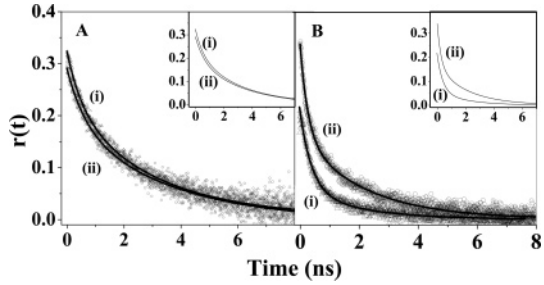

Figure 4. Fluorescence anisotropy decay of C480 in 1 wt % P123 along with fitted curve at (A) $\lambda_{ex} = 375$ nm ($\lambda_{em} = 440$ nm) and (B) $\lambda_{ex} = 435$ nm ($\lambda_{em} = 440$ nm): (i) in the absence (△) of CTAC and (ii) in the presence of 0.5 mM CTAC (○). Fitted curves of the decay are shown in the inset.

TABLE 2: Parameters of Anisotropy Decay of C480 in 1 wt % P123 in the Absence and Presence of 0.5 mM CTAC at Different λ_{ex}

			decay parameter of $r(t)$			
	r_0		P123		P123 + CTAC	
λ_{ex} (nm)	P123	P123 + CTAC	τ_{fast}[a] (ps) (a_{fast})	τ_{slow}[a] (ps) (a_{slow})	τ_{fast}[a] (ps) (a_{fast})	τ_{slow}[a] (ps) (a_{slow})
375	0.33	0.29	450 (0.25)	2750 (0.75)	630 (0.35)	3500 (0.65)
405	0.33	0.29	550 (0.25)	2550 (0.75)	600 (0.31)	3000 (0.69)
435	0.21	0.34	400 (0.75)	2050 (0.25)	270 (0.50)	2170 (0.50)

[a] ±5%.

and 3500 ps (65%). The corresponding values for $\lambda_{ex} = 435$ nm are 270 ps (50%) and 2170 ps (50%). Thus in a P123−CTAC aggregate the average rotational relaxation time decreases nearly 2-fold from 2500 ps at $\lambda_{ex} = 375$ nm to 1200 ps at $\lambda_{ex} = 435$ nm.

It should be noted that for $\lambda_{ex} = 375-435$ nm the average rotational relaxation time of C480 in a P123−CTAC aggregate is about 1.5 times longer than that in P123 micelle. This is in sharp contrast to the faster anisotropy decay in P123−SDS aggregates relative to P123 micelle.[6c] The faster rotational dynamics in P123−SDS aggregate may be ascribed to its smaller size (and faster tumbling) compared to the P123 micelle. Since the size of the P123−CTAC aggregate (core radius ∼ 3.5 nm, overall R ∼ 9 nm) is slightly smaller than that of P123 (core radius ∼ 4.2 nm, R ∼ 10 nm),[8a] the slower anisotropy decay in P123−CTAC is intriguing. It seems that penetration of CTAC with charged head groups and counterions increases local friction in P123−CTAC aggregate. The interaction of the probe (C480) with the charged head group and counterion offsets the effect of decrease in size.

It should also be noted the λ_{ex} dependence of the anisotropy decay in the case of P123−CTAC is larger than that in P123−SDS aggregate. With increase in λ_{ex}, the average rotational relaxation time of C480 in P123−CTAC decreases nearly 2 times from 2500 ps at 375 nm to 1200 ps at 435 nm. In contrast, P123−SDS displays a very small change (1.1 times) from 1200 to 1350 ps.[6c] This is presumably because penetration of the hydrophobic core of P123 micelle by SDS reduces the difference in the slow core (excited at 375 nm) and the fast corona region (excited at 435 nm).

3.3. Solvation Dynamics of C480 in P123 Micelle and in P123−CTAC Aggregate. Figures 5 and 6 shows the picosecond and femtosecond transients of C480 in P123 micelle in the presence and absence of 0.5 mM CTAC. In both P123 micelle and P123−CTAC complex, emission of C480 exhibits a rise at the red end of the emission spectrum and a decay at blue end. This is a clear signature of solvation dynamics. For $\lambda_{ex} = 375$ nm, in P123 micelle, the fluorescence decay at 410 nm (blue end) exhibits four decay components: 1, 30, 670, and 3500 ps. In P123−CTAC aggregate, the corresponding decay components are 7.8, 530, and 3200 ps and at 540 nm (red end) there are two rise components (3 and 1050 ps) with a long decay component (6400 ps). In P123 micelle, three rise components (1, 20, and 1020 ps) precede a very long decay component (6600 ps) at the same (540 nm) emission wavelength.

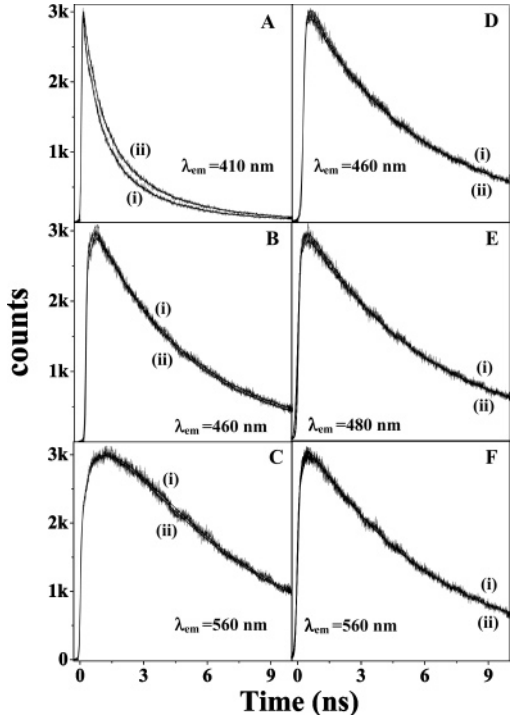

Figure 5. Picosecond decay of the C480 in 1 wt % P123 at $\lambda_{ex} = 375$ nm (A−C) and 435 nm (D−F). λ_{em} at (A) 410, (B) 460, (C) 560, (D) 460, (E) 480, and (F) 560 nm. (i) In the presence and (ii) in the absence of 0.5 mM CTAC.

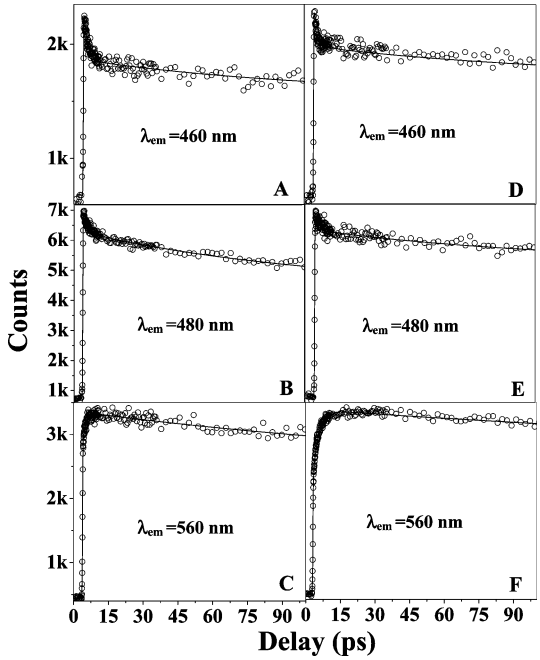

Figure 6. Femtosecond transients of C480 ($\lambda_{ex} = 435$ nm) in 1 wt % P123 in the absence of CTAC (A−C) and in the presence of 0.5 mM CTAC (D−F). λ_{em} at (A) 460, (B) 480, (C) 560, (D) 460, (E) 480, and (F) 560 nm.

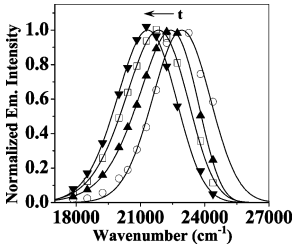

Figure 7. Time-resolved emission spectra (TRES) of C480 ($\lambda_{ex} = 375$ nm) in 1 wt % P123 in the presence of 0.5 mM CTAC at 0 ps (○), 700 ps (▲), 3500 ps (□), and 10 000 ps (▼).

For excitation at the red end ($\lambda_{ex} = 435$ nm), i.e., in the polar peripheral region, no long rise components (100−1000 ps) are detected. In P123−CTAC aggregate, at $\lambda_{em} = 460$ nm, there are two ultrafast decay components with time constants 2.3 and 100 ps along with a long decay component 5560 ps (Figures 5 and 6). This suggests that excitation at the red end selects molecules at a site (in peripheral region) where solvation dynamics is very fast and does not display any ultraslow component in 100−1000 ps time scale. In a P123 micelle, for $\lambda_{ex} = 435$ nm, the femtosecond transient of C480 at $\lambda_{em} = 560$ nm (red end) displays an ultrafast rise of 2.3 ps followed by two decay components of 400 and 6000 ps. In a P123−CTAC aggregate, the femtosecond transient at the red end ($\lambda_{em} = 560$ nm) displays an ultrafast rise component of 1.3 ps followed by two decay components 170 and 6100 ps. In P123 micelle ($\lambda_{ex} = 435$ nm), at the blue end ($\lambda_{em} = 460$ nm), there are two ultrafast decay components of 1.6 and 65 ps along with a long decay component of 5500 ps.

Figure 7 shows the time-resolved emission spectra (TRES) of C480 in a P123−CTAC self-assembly for $\lambda_{ex} = 375$ nm. From Table 3, it is evident that in both P123 micelle and in P123−CTAC aggregate the total dynamic Stokes shift, DSS = $\nu(0) - \nu(\infty)$, decreases 3−4 times as λ_{ex} increases from 375−435 nm. This implies that the solvation dynamics becomes faster with increase in λ_{ex}. For $\lambda_{ex} = 375$ nm, i.e., for the core region, almost the entire amount of solvation is captured. However, at a long λ_{ex}, a significant amount of solvation dynamics is missed even in our femtosecond set up. The amount of solvation missed may be calculated by using Fee−Maroncelli procedure.[12b] Figures 8 and 9 show the decays of solvent response function, $C(t)$, for different excitation wavelengths, and Table 3 summarizes the decay parameters of $C(t)$ along with DSS.

TABLE 3: Decay Parameters of $C(t)$ of C480 in 1 wt % P123 Micelle in the Presence and Absence of 0.5 mM CTAC at Different λ_{ex}

	$\Delta\nu_{obs}$[a] ($\nu(0)$) (cm^{-1})		decay parameter of $C(t)$, τ_i[c] (a_i) (ps)	
λ_{ex} (nm)	P123	P123 + CTAC	P123	P123 + CTAC
375	1850 (23440)	1600 (22930)	2 (7%), 130 (24%), 4000 (69%)	2 (7%), 60 (10%), 4000 (83%)
405	1350 (22580)	1450 (22590)	<0.3 (31%),[b] 2 (6%), 60 (10%), 3000 (53%)	<0.3 (16%),[b] 2 (2%), 20 (20%), 3000 (62%)
435	350 (21370)	400 (21230)	<0.3 (83%),[b] 2 (17%)	<0.3 (80%),[b] 2 (20%),

[a] ±100 cm^{-1}. [b] Calculated using Fee-Maroncelli Method.[12b] [c] ±10%.

From Figure 8 and 9 and Table 3, it is evident that for $\lambda_{ex} = 375$ nm the solvation dynamics in a P123 micelle displays a very fast (∼2 ps) component and a very long component (4000 ps) along with an intermediate component (130 ps). For $\lambda_{ex} = 375$ nm, in P123−CTAC aggregate, the decay components of $C(t)$ are 2, 60, and 4000 ps. With increase in λ_{ex}, the solvation

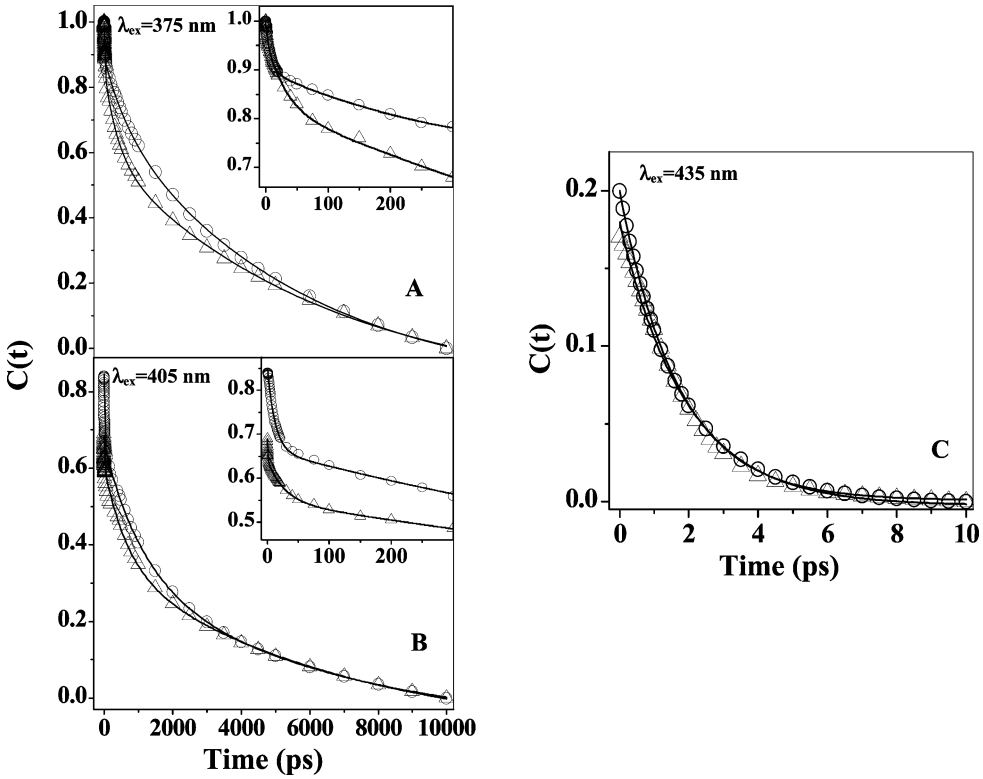

Figure 8. Complete decay of solvent response function $C(t)$ of C480 in 1 wt % P123 for (A) $\lambda_{ex} = 375$ nm, (B) $\lambda_{ex} = 405$ nm, and (C) $\lambda_{ex} = 435$ nm in the absence (△) and presence (○) of 0.5 mM CTAC. The points denote the actual values of $C(t)$ and the solid line denotes the best fit. Initial portions of the decays are shown in the inset.

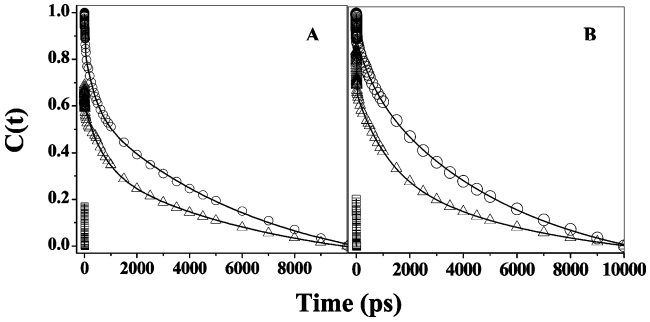

Figure 9. Complete decay of solvent response function $C(t)$ of C480 in 1 wt % P123 in the absence (A) and in the presence (B) of 0.5 mM CTAC: $\lambda_{ex} = 375$ (○), 405 (△), and 435 nm (□). The points denote the actual values of $C(t)$ and the solid line denotes the best fit.

dynamics becomes faster for both P123 micelle and P123−CTAC aggregate. For $\lambda_{ex} = 435$ nm, in both the systems, a major part of solvation dynamics is missed in our femtosecond set up (resolution 0.3 ps) and a 2 ps component is detected. In P123−CTAC, the contribution of the ultraslow component decreases gradually from 83% at $\lambda_{ex} = 375$ nm to 62% at $\lambda_{ex} = 405$ nm and finally disappears at $\lambda_{ex} = 435$ nm. Similarly, a sharp acceleration with solvation dynamics with increase in λ_{ex} and complete disappearance of the ultraslow components at $\lambda_{ex} = 435$ nm is also observed in P123 micelle (Figure 9 and Table 3).

It is evident that the ultrafast and ultraslow components of solvation dynamics remain similar in both P123−CTAC aggregate and P123 micelle. The main difference is observed in the intermediate component. For $\lambda_{ex} = 375$ nm, the intermediate component in P123−CTAC complex (60 ps) is about 2-fold faster than that in P123 micelle (130 ps). At $\lambda_{ex} = 405$ nm, the intermediate component is 20 ps in P123−CTAC and 60 ps in P123 micelle. Many previous experiments and simulations has suggested that a fast component (fifty to several hundred picoseconds) arises from polymer chain dynamics.[14−17] Following this, we assign the 60 ps component (in P123 micelle) to polymer chain dynamics. The polymer chain dynamics represents motion of the polar ends of the polymer chain (oxygen in PEO and PPO) and the associated water molecules. Insertion of CTAC inside P123 is likely to affect the polymer chain dynamics, and this is presumably responsible for the modification and eventually complete absence of this component (60 ps) at $\lambda_{ex} = 435$ nm in P123−CTAC. Note, in the case of P123−SDS[6c] because of the 10 times larger concentration of P123, the chain dynamics is much slower and a substantially large contribution (33%) of 200 ps component is detected even at $\lambda_{ex} = 435$ nm.[6c]

The ultraslow component (3000−4000 ps) observed in P123−CTAC (for $\lambda_{ex} = 375$ and 405 nm) is similar in time scale to those reported for polymer and polymer-surfactant aggregates.[18] The origin of this could be rupture of water−polymer hydrogen bond of quasi-bound water as envisaged by Nandi and Bagchi.[19] Such conversion of bound water to free water may also involve coherent motion of the polymer chain ("co-operative chain melting"). The other possible mechanism could be self-diffusion of the probe (C480) molecule from a nonpolar to polar region following excitation.[4a,20]

In summary, it is evident that with increase in λ_{ex} the anisotropy decay and solvation dynamics in P123−CTAC aggregate change quite remarkably. This is obviously due to distribution of the probes in different regions of P123−CTAC aggregate and P123 micelle. Excitation at the blue end (375 nm) selects the probe (C480) molecules in the relatively nonpolar and slower region near the core of the P123−CTAC aggregate, while excitation at 435 nm corresponds to the peripheral corona region.

It may be noted that the location dependent solvent relaxation is consistent with recent simulations of solvation dynamics in different regions of a protein.[21] Further, the position dependent solvation may affect polar reactions such as acid−base reactions. Very recently, using mixed quantum-classical simulation, Thompson showed that the free energy and entropy of proton transfer in a hydrophobic cavity depends on location.[22]

4. Conclusion

This work demonstrates that the P123−CTAC aggregate exhibits large REES (22 nm) and significant excitation wavelength dependence in anisotropy decay and solvation dynamics. This is assigned to different regions in this self-assembly. The solvation dynamics becomes 2−3 orders faster as λ_{ex} is increased from 375 to 435 nm. This is attributed to the difference between the highly restricted core region (excited at $\lambda_{ex} = 375$ nm) and the highly mobile corona region (excited at $\lambda_{ex} = 435$ nm). The differences in the anisotropy decay and solvation dynamics in P123−CTAC from those in P123−SDS aggregate are attributed to their structural differences.

Acknowledgment. Thanks are due to Department of Science and Technology, India (Project No. IR/I1/CF-01/2002 and J. C. Bose Fellowship) and Council of Scientific and Industrial Research (CSIR) for generous research grants. S.D., A.A., U.M., and S.G. thank CSIR for awarding fellowships. K.B. thanks Dr. P. K. Das for a gift of CTAC.

References and Notes

(1) (a) Alexandridis, P.; Holzwarth, J. F.; Hatton, T. A. *Macromolecules* **1994**, *27*, 2414. (b) da Silva, R. C.; Olofsson, G.; Schillen, K.; Loh, W. *J. Phys. Chem. B* **2002**, *106*, 1239.

(2) (a) Mortensen, K. *Macromolecules* **1997**, *30*, 503. (b) Goldmints, I.; von Gottberg, K.; Smith, K. A.; Hatton, T. A. *Langmuir* **1997**, *13*, 3659. (c) Wanka, G.; Hoffmann, H.; Ulbricht, W. *Macromolecules* **1994**, *27*, 4145.

(3) (a) Alexandridis, P. *Macromolecules* **1998**, *31*, 6935. (b) Alexandridis, P.; Olsson, U.; Lindman, B. *Langmuir* **1998**, *14*, 2627. (c) Ganguly, R.; Aswal, V. K.; Hassan, P. A.; Gopalakrishnan, I. K.; Yakhmi, J. V. *J. Phys. Chem. B* **2005**, *109*, 5653.

(4) (a) Sachl, R.; Stepanek, M.; Prochazka, K.; Humpolickova, J.; Hof, M. *Langmuir* **2008**, *24*, 288. (b) Humpolickova, J.; Stepanek, M.; Prochazka, K.; Hof, M. *J. Phys. Chem. A* ***2005***, *109*, 10803. (c) Kumbhakar, M.; Ganguly, R. *J. Phys. Chem. B* **2007**, *111*, 3935. (d) Mali, K. S.; Dutt, G. B.; Mukherjee, T. *J. Chem. Phys.* **2006**, *124*, 054904.

(5) (a) Grant, C. D.; DeRitter, M. R.; Steege, K. E.; Fadeeva, T. A.; Castner, E. W., Jr. *Langmuir* **2005**, *21*, 1745. (b) Grant, C. D.; Steege, K. E.; Bunagan, M. R.; Castner, E. W., Jr. *J. Phys. Chem. B* **2005**, *109*, 22273.

(6) (a) Sen, P.; Ghosh, S.; Sahu, K.; Mondal, S. K.; Roy, D.; Bhattacharyya, K. *J. Chem. Phys.* **2006**, *124*, 204905. (b) Ghosh, S.; Adhikari, A.; Mandal, U.; Dey, S.; Bhattacharyya, K. *J. Phys. Chem. C* **2007**, *111*, 8775. (c) Mandal, U.; Adhikari, A.; Dey, S.; Ghosh, S.; Mondal, S. K.; Bhattacharyya, K. *J. Phys. Chem. B* **2007**, *111*, 5896. (d) Adhikari, A.; Sahu, K.; Dey, S.; Ghosh, S.; Mandal, U.; Bhattacharyya, K. *J. Phys. Chem. B* **2007**, *111*.

(7) (a) Mondal, S. K.; Ghosh, S.; Sahu, K.; Mandal, U.; Bhattacharyya, K. *J. Chem. Phys.* **2006**, *125*, 224710. (b) Ghosh, S.; Dey, S.; Adhikari, A.; Mandal, U.; Bhattacharyya, K. *J. Phys. Chem. B* **2007**, *111*, 7085.

(8) (a) Jansson, J.; Schillen, K.; Nilsson, M.; Sodermano, O.; Fritz, G.; Bergmann, A.; Glatter, O. *J. Phys. Chem. B* **2005**, *109*, 7073. (b) Vangeyte, P.; Leyh, B.; Aubray, L.; Grandjean, J.; Misselyn-Baudin, A.-M.; Jerome, R. *Langmuir* **2004**, *20*, 9019. (c) Almgren, M.; Van Stam, J.; Lindblad, C.; Li, P.; Stilbs, P.; Bahadur, P. *J. Phys. Chem.* **1991**, *95*, 5677. (d) Jansson, J.; Schillen, K.; Olofsson, G.; da Silva, R. C.; Loh, W. *J. Phys. Chem. B* **2004**, *108*, 82.

(9) (a) Hecht, E.; Mortensen, K.; Gradzielski, M.; Hoffmann, H. *J. Phys. Chem.* **1995**, *99*, 4866. (b) Ganguly, R.; Aswal, V. K.; Hassan, P. A.; Gopalakrishnan, I. K.; Kulshreshtha, S. K. *J. Phys. Chem. B* **2006**, *110*, 9843.

(10) (a) Demchenko, A. P. *Biophys. Chem.* **1982**, *15*, 101. (b) Demchenko, A. P. *Luminescence* **2002**, *17*, 19. (c) Lakowicz, J. R. *Biochemistry*

1984, *23*, 3013. (d) Kelkar, D. A.; Chattopadhyay, A. *J. Phys. Chem. B* **2004**, *108*, 12151. (e) Mukherjee, S.; Chattopadhyay, A. *Langmuir* **2005**, *21*, 287.

(11) Vinogradov, A. M.; Tatikolov, A. S.; Costa, S. M. B. *Phys. Chem. Chem. Phys.* **2001**, *3*, 4325.

(12) (a) Maroncelli, M.; Fleming, G. R. *J. Chem. Phys.* **1987**, *86*, 6221. (b) Fee, R. S.; Maroncelli, M. *Chem. Phys.* **1994**, *183*, 235.

(13) Jones, G., II; Jackson, W. R.; Choi, C.-Y.; Bergmark, W. R. *J. Phys. Chem.* **1985**, *89*, 294.

(14) (a) Shirota, H.; Segawa, H. *J. Phys. Chem. A* **2003**, *107*, 3719. (b) Shirota, H. *J. Phys. Chem. B* **2005**, *109*, 7053.

(15) (a) Shirota, H.; Tamoto, Y.; Segawa, H. *J. Phys. Chem. A* **2004**, *108*, 3244. (b) Corbeil, E. M.; Riter, R. E.; Levinger, N. E. *J. Phys. Chem. B* **2004**, *108*, 10777. (c) Tan, H.-S.; Piletic, I. R.; Riter, R. E.; Levinger, N. E.; Fayer, M. D. *Phys. Rev. Lett.* **2005**, *94*, 057405.

(16) (a) Olander, R.; Nitzan, A. *J. Chem. Phys.* **1995**, *102*, 7180. (b) Argaman, R.; Huppert, D. *J. Phys. Chem. A* **1998**, *102*, 6215. (c) Pant, D.; Levinger, N. E. *Langmuir* **2000**, *16*, 10123.

(17) (a) Pal, S. K.; Peon, J.; Bagchi, B.; Zewail, A. H. *J. Phys. Chem. B* **2002**, *106*, 12376. (b) Srinivas, G.; Sebastian, K. L.; Bagchi, B. *J. Chem. Phys.* **2002**, *116*, 7276.

(18) (a) Frauchiger, L.; Shirota, H.; Uhrich, K. E.; Castner, E. W., Jr. *J. Phys. Chem. B* **2002**, *106*, 7463. (b) Sen, S.; Sukul, D.; Dutt, P.; Bhattacharyya, K. *J. Phys. Chem. B* **2002**, *106*, 3763.

(19) (a) Nandi, N.; Bagchi, B. *J. Phys. Chem. A* **1997**, *101*, 10954. (b) Nandi, N.; Bagchi, B. *J. Phys. Chem. B* **1998**, *102*, 8217.

(20) (a) Thompson, W. H. *J. Chem. Phys.* **2004**, *120*, 8125. (b) Faeder, J.; Ladanyi, B. M. *J. Phys. Chem. B* **2005**, *109*, 6732.

(21) (a) Bandyopadhyay, S.; Chakraborty, S.; Balasubramanian, S.; Bagchi, B. *J. Am. Chem. Soc.* **2005**, *127*, 4071. (b) Abel, S.; Waks, M.; Urbach, W.; Marchi, M. *J. Am. Chem. Soc.* **2006**, *128*, 382. (c) Jana, B.; Pal, S.; Maiti, P. K.; Lin, S. T.; Hynes, J. T.; Bagchi, B. *J. Phys. Chem. B* **2006**, *110*, 19611.

(22) (a) Thompson, W. H. *J. Phys. Chem. B* **2005**, *109*, 18201. (b) Mitchell-Koch, K. R.; Thompson, W. H. *J. Phys. Chem. C* **2007**, *111*, 11991.